

Article

Introduction of Al into the HPM-1 Framework by In Situ Generated Seeds as an Alternative Methodology

Paloma Vinaches ¹ , Alex Rojas ², Ana Ellen V. de Alencar ¹ , Enrique Rodríguez-Castellón ³ ,
Tiago P. Braga ¹  and Sibe B. C. Pergher ^{1,*}

¹ Laboratório de Peneiras Moleculares (LABPEMOL), Instituto de Química, Universidade Federal de Rio Grande do Norte, Campus de Lagoa Nova, 59078-970 Natal, Brazil; palomavinaches@gmail.com (P.V.); ellenvalencar@yahoo.com.br (A.E.V.d.A.); tiagoquimicaufn@gmail.com (T.P.B.)

² Instituto Federal do Maranhão (UFMA), Avenida dos Portugueses, Vila Bacanga, 65080-805 São Luís, Brazil; alex1981rojas@hotmail.com

³ Departamento de Química Inorgánica, Cristalografía e Mineralogía, Facultad de Ciencias, Universidad de Málaga (UMA), 29071 Málaga, Spain; castellon@uma.es

* Correspondence: sibepergher@gmail.com; Tel.: +55-84-3342-2323

Received: 10 July 2018; Accepted: 29 July 2018; Published: 13 September 2018



Abstract: An alternative method for the introduction of aluminum into the STW zeolitic framework is presented. HPM-1, a chiral STW zeolite with helical pores, was synthesized in the pure silica form, and an aluminum source was added by in situ generated seeds. Displacements of the peak positions in the Al samples were found in the X-ray diffractograms, indicating the possible incorporation of the heteroatom into the framework. Using an analysis of the ²⁹Si and ²⁷Al magic-angle spinning nuclear magnetic resonance (MAS NMR) spectra, we concluded that the aluminum was effectively introduced into the framework. The (Al_{TETRAHEDRAL}/Al_{OCTAHEDRAL}) ratio and its textural properties were studied to explain the catalytic ethanol conversion results at medium temperatures. The sample with the lowest Si/Al ratio showed the best results due to its higher surface area and pore volume, in comparison to those observed for the sample with the highest Si/Al ratio, and due to its higher bulk tetrahedral aluminum content, in comparison to the intermediate Si/Al ratio sample. All catalysts were selective to ethylene and diethyl ether, confirming the presence of acidic sites.

Keywords: STW zeolite; aluminosilicate; seeds; 2-ethyl-1,3,4-trimethylimidazolium; hydrofluoric media; ethanol dehydration

1. Introduction

Historically, zeolites have been defined as crystalline porous aluminosilicates, consisting of tetrahedra in which Si⁴⁺ or Al³⁺ cations are found inside and O²⁻ anions are placed at their vertices [1,2]. Owing to the increasing knowledge of the zeolitic structure, the current definition has evolved to be, crystalline porous materials for which the structures are formed by tetrahedra enclosing a variety of cations in the interior and with O²⁻ anions at the tetrahedral vertices [3].

HPM-1 is a pure Si chiral STW zeolite with helical pores [4]. Its tridimensional channel system can be decomposed into double 4-ring (D4R) units and [4⁶5⁸8²10²] cavities, forming 10-ring helical channels connected by straight 8-ring pores [5,6]. This structure is shown in Figure 1. The zeolite was obtained from the organic structure of the directing agent 2E134TMI (2-ethyl-1,3,4-trimethylimidazolium). These chiral zeolites have become a focus of study for the last few years [7,8]. The importance of synthesizing these structures arises from their application in the petroleum industry and from their use in obtaining chirally pure drugs.

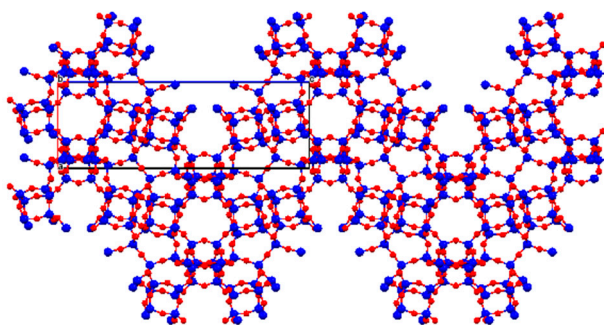
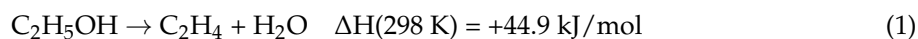


Figure 1. Representation of the STW topology obtained thanks to the .cif from the IZA Database website (with permission from Reference [9], copyright © 2018 Structure Commission of the International Zeolite Association (IZA-SC) [9]) using the Mercury program [10].

Recently, the incorporation of aluminum (Si/Al = 107) in its non-calcined structure was reported, and the obtained structure was named high silica HPM-1 [5]. This material already shows catalytic properties in the isobutene isomerization, which demonstrates its high selectivity. The germanoaluminosilicate was also synthesized by Brand et al. [11] who achieved enantiomeric enrichment. However, a literature search revealed that the calcined aluminosilicate has not been previously described, as only the characterizations of the as-synthesized samples were presented. However, there is interest for understanding its application in catalysis.

Ethanol dehydration is used as a model reaction to confirm the existence of acidic sites [12]. At low reaction temperatures, the main products are ethylene and diethyl ether [13]. The generation of the former product is due to an endothermic reaction (Equation (1)), which is favored thermodynamically at moderate temperatures [14,15].



The second reaction (Equation (2)) is an exothermic reaction resulting in competition between the two products.



As previously mentioned, HPM-1 was obtained as a pure aluminosilicate by the traditional methods of heteroatom introduction in addition to the incorporation of a low quantity of aluminum prior to calcination. Therefore, further study is necessary to understand the behavior of this structure to facilitate the incorporation of different heteroatoms to optimize the synthesis process. For this purpose, the present work aims to study an alternative strategy of Al incorporation and is based on Moura et al.'s published work on the addition of Al into the magadiite framework [16].

2. Materials and Methods

Synthetic procedures: The reagents used in the synthesis were tetraethylorthosilicate (TEOS, 98%, Sigma-Aldrich, St. Louis, MO, USA), aluminum hydroxide (62.23%, Synth, Diadema, SP, Brazil, Al(OH)₃), 2-ethyl-1,3,4-methylimidazolium hydroxide (2E134TMIOH, synthesized), hydrofluoric acid (40%, Sigma-Aldrich, St. Louis, MO, USA), and distilled water.

The cation 2E134TMIOH was synthesized according to the procedure described by Rojas et al. [4]. The synthesis of HPM-1 incorporating aluminum was a variation of the pure silica procedure, and was adapted by the process, reported by Moura et al. [16], to incorporate Al into the lamellar silicate magadiite. In this way, the cation 2E134TMIOH was concentrated up to 1 g/L. Subsequently, TEOS was added to the concentrated cation solution and was left to hydrolyze until the desired 33H₂O/SiO₂ ratio was reached (due to the ethanol and water evaporation). This procedure was followed according to

the weight changes, that is, the weight lost was considered to be ethanol and water evaporation. Once the desired $\text{SiO}_2/2\text{E134TMIOH}/\text{H}_2\text{O}$ composition was reached, HF was added and mixed manually for approximately 10–15 min. The gel composition at this point of synthesis was $\text{SiO}_2: x \text{Al}_2\text{O}_3: 0.5 \text{SDAOH}: 0.5 \text{HF}: 4.7 \text{H}_2\text{O}$, where $x = 0$ (as no aluminum was added yet). Then, the synthesis gel was divided among several Teflon autoclaves that were placed within their respective steel autoclaves. These autoclaves were placed into a rotatory oven at 175 °C for 3 days. At this time, some of the autoclaves were cooled, and the amount of SiO_2 per autoclave was calculated, according to the amount that the synthesis gel weighed. Using the amount of silica per autoclave as a reference, it was possible to calculate the amount of $\text{Al}(\text{OH})_3$ needed per autoclave. Further, $\text{Al}(\text{OH})_3$ was added to attain the desired compositions ($x = 0.015, 0.025, \text{ and } 0.035$). After this, the autoclaves were placed in rotation again at 175 °C for 1 more day. The products were then filtered under a vacuum and washed with an abundance of distilled water. The pH of the initial gel, at the time of aluminum introduction, was 7, and the pH at the end of the synthesis was 8, but it decreased again to 7 when the product was washed. Finally, the samples were calcined at 550 °C for 6 h. This process is summarized in Figure S1 (Supplementary Material).

Characterization: The samples were analyzed by XRD (Bruker D2-Phaser, Bruker, Billerica, MA, USA, with a Lynxeye detector and Cu radiation, using a divergent slit of 0.6 mm, a central slit of 1 mm, a measuring step of 0.004° , and an acquisition time of 0.5 s) to identify the compounds and their crystalline structure. Calibration of the instrument was performed using a National Institute of Standards and Technology (NIST) corundum standard for every measurement in order to ensure that all the samples were comparable. The samples were also analyzed by X-ray fluorescence (XRF, EDX-720/800 HS, Shimadzu, Kyoto, Japan) to calculate the total Si/Al ratio (including Al_{TETRA} and Al_{OCTA}). Magic-angle spinning solid-state nuclear magnetic spectroscopy (MAS NMR) was used to calculate the actual Si/ Al_{TETRA} ratio of the framework and the $\text{Al}_{\text{TETRA}}/\text{Al}_{\text{OCTA}}$ ratio of the samples. The ^{29}Si and ^{27}Al MAS NMR spectra were recorded using a Bruker AVIII HD 600 NMR spectrometer (Bruker, Billerica, MA, USA) (with a field strength of 14.1 T) at 156.4 MHz with a 2.5 mm triple-resonance DVT probe that used zirconia rotors at the spinning rates of 15 kHz (^{29}Si) and 20 kHz (^{27}Al). The ^{29}Si experiments were performed with proton decoupling (cw (continuous wave) sequence) by applying a single pulse ($\pi/2$), an excitation pulse of 5 μs , and a 60 s relaxation delay to obtain 10,800 scans. The ^{27}Al experiments were also performed with proton decoupling (cw sequence) by applying a single pulse ($\pi/12$), an excitation pulse of 1 μs , and a 5 s relaxation delay to obtain 200 scans. The chemical shifts were referenced to an external solution of tetramethylsilane (TMS) and to an external solution of 1 M of $\text{Al}(\text{NO}_3)_3$ for ^{29}Si and ^{27}Al , respectively. Field Emission Gun Scanning Electron Microscopy (MIRA3 FEG-SEM, Tescan, Brno, Czech Republic) was used to study the morphology of the samples synthesized with aluminum. The samples were studied by XPS (X-ray photoelectron spectroscopy, Physical Electronics PHI-750 spectrometer, Physical Electronics, Chanhassen, MN, USA) with an X-ray radiation source of Mg $K\alpha$ (1253.6 eV) and referenced to as C 1s (284.8 eV) to characterize the Si/ Al_{TETRA} ratio and the Al state at the surface. Finally, to study the textural properties of the samples, the calcined samples were pretreated at 200 °C under a vacuum overnight in a Micromeritics Asap 2020 (Micromeritics, Norcross, GA, USA) and were examined using nitrogen as a probe molecule.

Ethanol dehydration: The ethanol used in this reaction was obtained from Sigma-Aldrich.

An amount of 0.1 g of each catalyst was activated at 350 °C and at atmospheric pressure for an hour in an N_2 atmosphere. The catalytic tests were performed in a fixed-bed flow reactor at atmospheric pressure and at 250 °C. A mixture containing N_2 and ethanol vapor (25 mL/min) was stabilized using drag gas (N_2) through a steam saturator system containing ethanol at 25 °C. The outlet gases were analyzed by gas chromatography (GC, Clarus 680, Perkin Elmer, Waltham, MA, USA) equipped with a flame ionization chamber (FIC) and a capillary column.

The ethanol conversion [12] is defined by Equation (3):

$$\%X(\text{EtOH}) = (N(\text{EtOH}_{\text{in}}) - N(\text{EtOH}_{\text{out}})) / (N(\text{EtOH}_{\text{in}})) \times 100 \quad (3)$$

For each product, the selectivity [12] can be calculated using Equation (4):

$$\%S(\text{Product } i) = N(\text{Product } i) / (\sum_0^i N(\text{Product } i)) \times 100 \quad (4)$$

3. Results and Discussion

The samples were obtained by hydrothermal synthesis after four days at 175 °C. The aluminum was added after the third day of synthesis, and the samples were then returned to the oven for the fourth day of heating. Afterwards, the samples were calcined at 550 °C. The complete synthesis is described in the Materials and Methods section, and the Si/Al ratios of the products are summarized in Table 1. The total Si/Al ratio of the products was initially measured by the XRF technique, and the results were similar to the Si/Al ratio of the synthesis gel.

Table 1. Obtained products.

Sample	Si/Al Synthesis Gel (Calculated)	Si/Al Products (XRF)
SiAl15	15	19.4
SiAl25	25	25.4
SiAl35	35	38.0
Pure_Silica	∞	∞

X-ray diffraction (XRD) experiments of the calcined samples were performed to prove that HPM-1 was obtained (Figures 2 and 3). To improve the visibility, the diffractograms were slightly shifted in their intensity. The Pure_Silica sample demonstrates the reproducibility of the original synthesis [4] and is used as the reference for comparison to the other obtained samples.

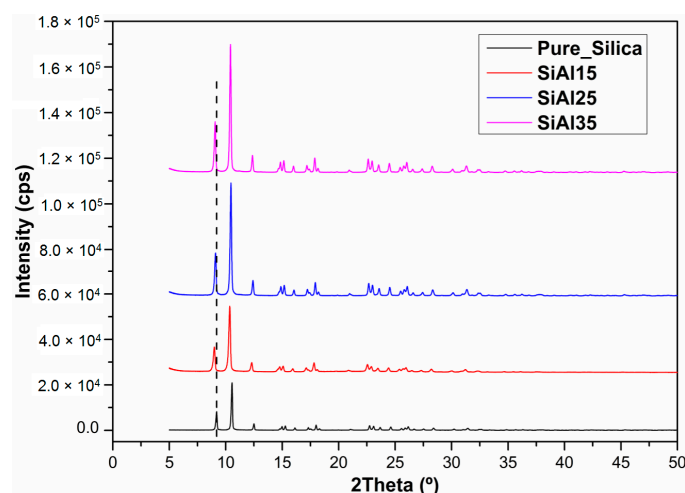


Figure 2. X-ray diffractograms of the calcined products.

It is possible to compare the peak positions of the samples as an indication of the incorporation of a heteroatom in the framework [17]. The substitution of an atom by a different atom in the unit cell results in a distortion of the cell parameters, owing to its different characteristics (e.g., volume, charge). Since the Bragg reflections of an X-ray diffractogram correspond to the different planes and atomic positions, a slight change in these positions, or atomic substitutions, will be reflected in the displacement of the 2θ values of the peaks. In this case, we are studying the incorporation of

aluminum, so a shift to lower 2θ values, relative to those of the pure silica samples, indicates that aluminum was effectively incorporated into the framework. Figure 3 shows the 2θ region between 8° and 13° , confirming that this displacement did occur in the three samples when Al was added, possibly suggesting that the aluminum entered the zeolitic framework. As expected, the SiAl15 sample with the highest quantity of Al added showed the largest shift in the diffractogram. Nevertheless, this observation still needs to be confirmed by other techniques because it is difficult to quantify the Si/Al_{TETRA} ratio with the X-ray diffractograms alone.

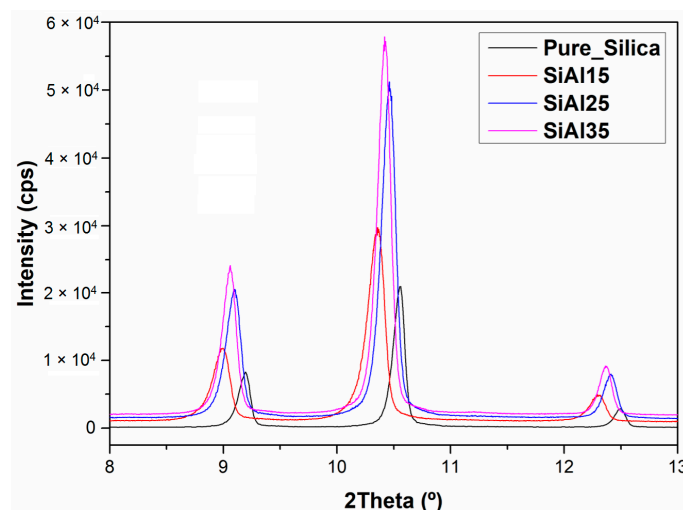


Figure 3. Magnified view of the X-ray diffractograms of the calcined samples.

The difference in the intensities of the same peak positions, among the samples, was another interesting observation from the X-ray diffractograms. These intensity values were normalized to create the average relative crystallinity index, with the number one assigned to the highest intensity of the four peaks at the same 2θ range. To obtain the average, the peak intensities were measured in the following 2θ ranges, $10.3\text{--}10.5^\circ$, $12.3\text{--}13.5^\circ$, $16.6\text{--}16.3^\circ$, and $24.1\text{--}24.8^\circ$. The results are shown in Table 2. Comparing the aluminosilicate samples, a lower quantity of aluminum in the synthesis helped to obtain a higher average crystallinity index. Surprisingly, the Pure_Silica sample showed the opposite behavior, probably because the presence of aluminum influenced its nucleation and the growth procedure was accelerating it. These results do not mean that the samples are amorphous; this is just a comparison among them as previously reported in the literature [18].

Table 2. Relative crystallinity index.

Sample	Average Relative Crystallinity Index
SiAl15	0.62
SiAl25	0.97
SiAl35	1.00
Pure_Silica	0.34

Studying the magic-angle spinning (MAS) NMR spectra of the calcined solids can provide more precise information on the Si and Al states, since this technique can calculate the Si/Al ratio, assuming that it is larger than seven (proven later). Therefore, the samples synthesized with aluminum were analyzed with this technique, as described by Pace [12]. Two different regions were observed in the ^{29}Si MAS NMR spectra of the calcined samples, which were synthesized with aluminum (Figure 4a, Table 3). This includes the chemical environment, at approximately 105 ppm to 120 ppm, in which all Si atoms, surrounded by O atoms, were bonded to four additional Si atoms. Additionally, the second

region centered at approximately 102 ppm which corresponds to the $\text{Si}[\text{OSi}]_3[\text{OAl}]$ species, that is, with one Al atom replacing one of the Si atoms in the second coordination sphere [4,12]. The bands of the first region were assigned to $\text{Si}[\text{OSi}]_4$ outside of the D4R cages (at approximately -115.5 ppm) and to $\text{Si}[\text{OSi}]_4$ in the D4R cages (at approximately 109 ppm) [19]. Comparing these chemical shifts with those reported for pure silica (published in [4,19]), a slight displacement, which is typical of the heteroatom introduction in a pure silica zeolite, was observed. In addition, the $\text{Si}[\text{OSi}]_3[\text{OAl}]$ species in the pure silica sample, confirming the introduction of aluminum in the framework, was not identified. This absence was reported previously for the pure silica form synthesized that employed HF and is explained as being due to the lack of connectivity defects after calcination [19,20]. The sample with the highest $\text{Si}/\text{Al}_{\text{TETRA}}$ ratio corresponded to the sample synthesized with the highest $(\text{Si}/\text{Al})_{\text{GEL}}$ ratio.

The ^{27}Al MAS NMR spectra (Figure 4b, Table 3) of the calcined samples also confirmed the existence of the aluminum framework, corresponding to the tetrahedral aluminum represented by the band at approximately 60 ppm. A band at approximately 7 ppm, related to octahedral aluminum, also appeared, with a variation in the intensity among the samples. These results showed that a higher aluminum concentration in the synthesis gel led to a lower content of bulk octahedral aluminum.

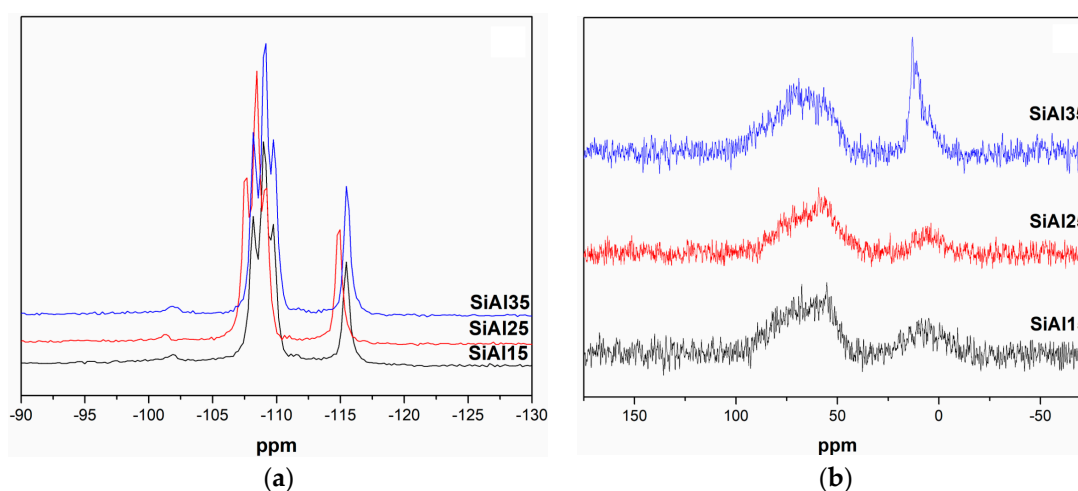


Figure 4. ^{29}Si (a) and ^{27}Al (b) MAS NMR (Magic-angle spinning solid-state nuclear magnetic spectroscopy) spectra of the calcined samples.

Table 3. ^{29}Si MAS NMR (Magic-angle spinning solid-state nuclear magnetic spectroscopy) chemical shifts of the calcined samples SiAl15, SiAl25, and SiAl35.

Sample	$\text{Si}/\text{Al}_{\text{TETRA}}$		$\text{Al}_{\text{TETRA}}/\text{Al}_{\text{OCTA}}$	
	MAS NMR	XPS	MAS NMR	XPS*
SiAl15	185.0	7.7	1.6	0.6
SiAl25	192.6	11.1	1.3	1.1
SiAl35	192.3	11.9	0.9	1.1

The three [Al] HPM-1 samples were also studied by X-ray photoelectron spectroscopy (XPS) because this technique provides fundamental information regarding the surface chemistry for catalytic reactions [21]. This technique had never previously been reported to study the aluminum distribution in HPM-1, as far as we know. Several interesting differences were found among the samples. Figure 5 presents the Al $2p$ signals from each sample, showing differences in the binding energy (BE, eV) values among the samples. These variations were in the range of the beta zeolite (differences of about ± 0.5 eV in BE), a topology that also presents a chiral polymorph [22]. The different $(\text{Si}/\text{Al}_{\text{TETRA}})_{\text{SURFACE}}$ ratios were calculated from these spectra and the Si $2p$ spectrum (Table 3). The results followed the same tendency as the ^{29}Si MAS NMR spectra, and showed that the surface was richer than the bulk in Al,

resulting in a higher amount of Al incorporated in the external layer of the zeolite. This measurement could also be taking the octahedral aluminum into account. Therefore, the $(Al_{TETRA}/Al_{OCTA})_{SURFACE}$ ratio was calculated, and the modified Auger parameter of Al (α') [23], from the different samples, was obtained according to Equation (5):

$$\alpha' = 1253.6 + KE(Al_{KLL}) - KE(Al\ 2p) \tag{5}$$

where $KE(Al_{KLL})$ is the kinetic energy of the Auger electron at Al_{KLL} (Figure 6), and $KE(Al\ 2p)$ is the kinetic energy of the Al 2p photoelectron. A comparison of these results with the results of ^{27}Al MAS NMR shows that, for SiAl25 and SiAl35, it is similarly indicated that the tetrahedral aluminum would be easily accessible as acidic sites. In the case of SiAl15, the octahedral aluminum content may interfere with the accessibility of the tetrahedral aluminum in future reactions. Despite the increasing ratio from SiAl15 to SiAl35, the results were as expected. The octahedral aluminum was outside of the framework; it was placed on the surface. The data obtained from the XPS analysis are summarized in Tables 3 and 4.

Table 4. XPS (X-ray photoelectron spectroscopy) results of the calcined samples.

Sample	Binding Energy Si 2p (eV)	Binding Energy Al 2p (eV)	α' Al _{TETRA} (eV)	α' Al _{OCTA} (eV)
SiAl15	102.6	74.5	1458.4	1460.8
SiAl25	103.7	75.0	1457.2	1460.2
SiAl35	102.7	74.0	1458.4	1459.8

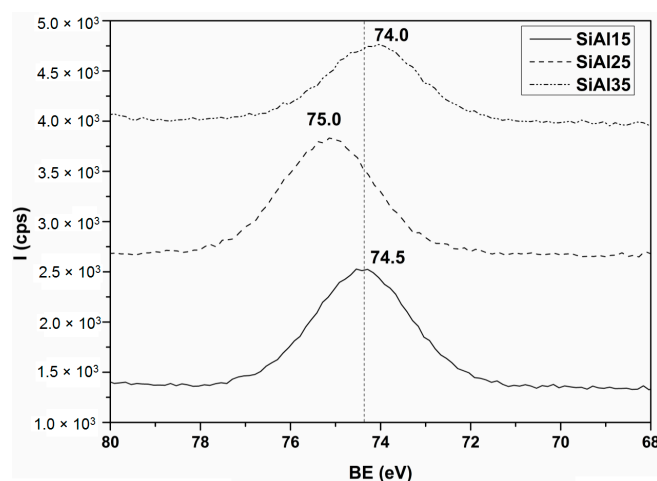


Figure 5. Al 2p signals of the calcined samples (XPS spectra).

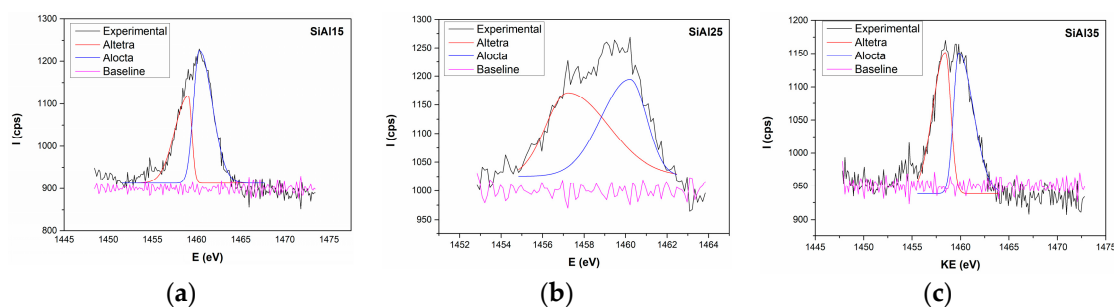


Figure 6. Al_{KLL} signals of the calcined samples (XPS spectra): (a) SiAl15; (b) SiAl25, and (c) SiAl35.

The SiAl25 sample was observed using field emission gun scanning electron microscopy (FEG-SEM), the obtained micrograph is shown in Figure 7, and the Supplementary Material in Figure S2.

The resulting morphology is similar to a rice grain, which has the same reported morphology for the pure silica HPM-1 [4].

Finally, to determine the acidic or basic character of the zeolite, the ethanol dehydration model reaction was used [12]. Figure 8 and Table 5 show the catalytic performance of the [Al] HPM-1 samples. Comparing all the samples, a greater ethanol conversion value was observed for the SiAl25 sample, and lower conversions were observed for the SiAl15 and SiAl35 samples. This order of conversion performance was explained by several factors. The first factor is the BET (Brunauer-Emmett-Teller) area (SBET, Table 5, Supplementary Material Figures S3–S5, and Tables S1–S3), which is directly related to the highest conversion values, because the highest SBET allows a higher quantity of accessible acidic sites [12]. Therefore, SiAl25 and SiAl35 were expected to show higher conversion values than SiAl15. The second factor influencing the ethanol conversion was the amount of octahedral aluminum. While SiAl15 had the highest Si/Al_{TETRA} ratio, its (Al_{TETRA}/Al_{OCTA})_{XPS} ratio was low, implying that the total pore volume (TPV, Table 5, Supplementary Material Tables S1–S3) was lower than in the other cases, thus preventing interaction between the ethanol and the active sites and making the diffusion of the molecules in the pores more difficult. The difference in the conversion performance between SiAl25 and SiAl35 was due to the bulk tetrahedral aluminum content, which was greater for SiAl25 than for SiAl35. Finally, even though SiAl35 has double the area of SiAl15, they presented a similar conversion value, probably because the higher area value was in consideration of the area of the octahedral aluminum, and did not interfere with the reaction. The Pure_Silica sample was also tested for the dehydration of ethanol and showed a very low activity (approximately 2–12%), which is practically inactive, owing to the minimal amount of Si-OH sites reported in a fluoride medium [4,12,19,20].

It is well known that the product selectivity in ethanol conversion is directly related to the acid strength of the material [24]. For the study of sample selectivity at 250 °C, ethanol was catalytically converted via the intramolecular and intermolecular dehydration reactions [25] to produce ethylene and diethylether (DEE), respectively (Table 5, Figure 8)—products that are only formed at acidic sites. This result demonstrated the high acidic character of the samples; the SiAl25 sample was the most acidic sample. Comparing the three cases, at a high temperature and conversion, DEE is produced with high selectivity, as expected, due to the exothermic nature of the reaction [14,15]. The differences in the observed selectivities were small and probably related to the quantity of the available acidic sites because the selectivity results appeared to follow the same pattern.

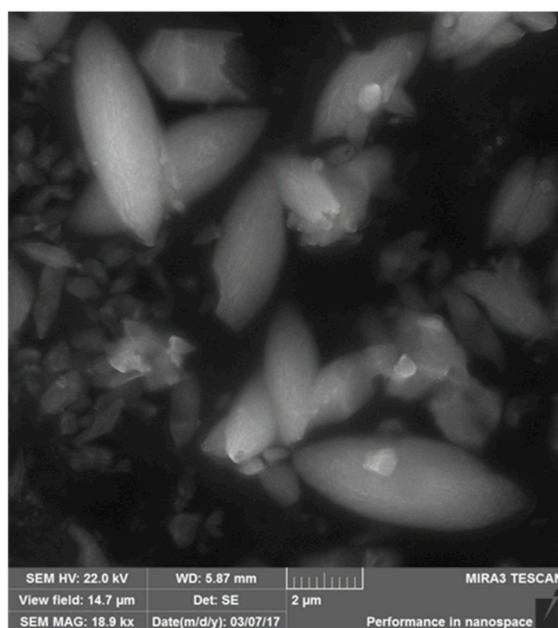


Figure 7. Micrograph of calcined sample SiAl25.

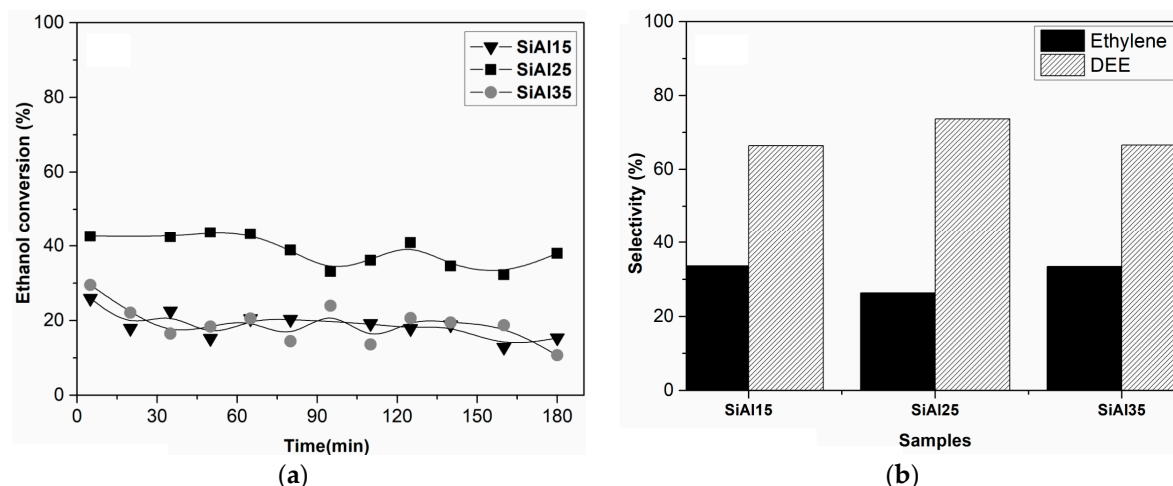


Figure 8. (a) Ethanol conversion as a function of time at 250 °C of the calcined [Al] HPM-1 samples and (b) product selectivity.

Table 5. Textural and catalysis results of the calcined samples SiAl15, SiAl25, and SiAl35.

Sample	Conversion (Media, %)	Selectivity—Ethylene (%)	Selectivity—DEE (%)	SBET (m ² g ⁻¹)	TPV * (cm ³ g ⁻¹)
SiAl15	20	33.6	66.4	332	0.19
SiAl25	38	26.3	73.7	631	0.26
SiAl35	20	33.4	66.6	623	0.26

* TPV (total pore volume) included the mesopore volume due to the space between particles. DEE: Diethylether. SBET: Brunauer-Emmett-Teller area.

4. Conclusions

This work studied a different method for the introduction of Al in the HPM-1 framework using in situ generated seeds. Three samples of [Al] HPM-1 were studied after calcination: SiAl15, SiAl25, and SiAl35. In every case, the SiAl15 product had the lowest Si/Al_{TETRA} ratio, but also had the lowest average crystallinity index and the lowest (Al_{TETRA}/Al_{OCTA})_{XPS} of the samples with aluminum. SiAl25 and SiAl35 had similar Si/Al_{TETRA} ratios, even though SiAl35 had more bulk octahedral aluminum. All samples were active for ethanol dehydration, with SiAl25 being the most active because it had the highest values of S_{BET}, the highest total pore volume, and a higher bulk tetrahedral aluminum content than that of SiAl35. The three catalysts were active to ethanol dehydration, therefore implying that they contained acidic sites. The selectivity results also demonstrated that ethylene production manifests the influence of the Al_{TETRA} acidic sites.

Supplementary Materials: The following are available online at <http://www.mdpi.com/2076-3417/8/9/1634/s1>, Figure S1: Scheme of the synthesis, Figure S2: SEM/EDX mapping of the sample SiAl25, Figure S3: Nitrogen sorption isotherm (SiAl15), Table S1: Textural analysis of the calcined sample SiAl15, Figure S4: Nitrogen sorption isotherm (SiAl25), Table S2: Textural analysis of the calcined sample SiAl25, Figure S5: Nitrogen sorption isotherm (SiAl35), Table S3: Textural analysis of the calcined sample SiAl35.

Author Contributions: Conceptualization and Methodology, P.V., A.R. and S.B.C.P.; Synthesis, P.V. and A.R.; Characterization, P.V., A.R., E.R.-C. and S.B.C.P.; Catalysis, P.V., A.E.V.d.A. and T.P.B.; Writing, P.V., A.R., A.E.V.d.A., E.R.-C., T.P.B. and S.B.C.P.

Funding: This research was funded by CAPES (Brazil), MINECO (Spain) project number CTQ2015-68951-C3-3-R, and FEDER funds.

Acknowledgments: The authors acknowledge PPGCEM, UFRN, UERN and UMA for the installations and financial support. The authors are also grateful to LABPEMOL (Laboratório de Peneiras Moleculares, UFRN) for the installations for the synthesis, catalysis and the XRD technique, UMA for the MAS NMR and XPS techniques, UERN Chemistry Department for the FEG-SEM micrographs, XRF-DEMAT (Laboratório de Caracterização Estrutural de Materiais, Departamento de Engenharia de Materiais, UFRN) for the XRF data, and the Institute of Chemistry (UFRN) for the IR technique.

Conflicts of Interest: The authors declare no conflict of interest. The funders had no role in the design of the study; in the collection, analyses, or interpretation of data; in the writing of the manuscript, and in the decision to publish the results.

References

1. Flanigen, E.M. Chapter 2 zeolites and molecular sieves an historical perspective. In *Studies in Surface Science and Catalysis*; van Bekkum, H., Flanigen, E.M., Jansen, J.C., Eds.; Elsevier: Amsterdam, The Netherlands, 1991; Volume 58, pp. 13–34.
2. Mintova, S.; Barrier, N. *Verified Synthesis of Zeolitic Materials*, 3rd ed.; Elsevier (On behalf of the Synthesis Commission of the International Zeolite Association): Amsterdam, The Netherlands, 2016; p. 405.
3. Cambor, M.A.; Hong, S.B. Synthetic silicate zeolites: Diverse materials accessible through geoinspiration. In *Porous Materials*; Bruce, D.W., O'Hare, D., Walton, R.I., Eds.; John Wiley & Sons, Ltd.: Hoboken, NJ, USA, 2010.
4. Rojas, A.; Arteaga, O.; Kahr, B.; Cambor, M.A. Synthesis, structure, and optical activity of HPM-1, a pure silica chiral zeolite. *J. Am. Chem. Soc.* **2013**, *135*, 11975–11984. [[CrossRef](#)] [[PubMed](#)]
5. Jo, D.; Hong, S.B.; Cambor, M.A. Monomolecular skeletal isomerization of 1-butene over selective zeolite catalysts. *ACS Catal.* **2015**, *5*, 2270–2274. [[CrossRef](#)]
6. Jo, D.; Lee, K.; Park, G.T.; Hong, S.B. Acid site density effects in zeolite-catalyzed 1-butene skeletal isomerization. *J. Catal.* **2016**, *335*, 58–61. [[CrossRef](#)]
7. Davis, M.E. Zeolites from a materials chemistry perspective. *Chem. Mater.* **2014**, *26*, 239–245. [[CrossRef](#)]
8. Bueno-Perez, R.; Balestra, S.R.G.; Cambor, M.A.; Min, J.G.; Hong, S.B.; Merklings, P.J.; Calero, S. Influence of flexibility on the separation of chiral isomers in STW-type zeolite. *Chem. A Eur. J.* **2018**, *24*, 4121–4132. [[CrossRef](#)] [[PubMed](#)]
9. Baerlocher, C.; McCusker, L.B. International Zeolite Association. Database of Zeolite Structures. 2007. Available online: <http://www.iza-structure.org/databases/> (accessed on 23 July 2018).
10. Macrae, C.F.; Edgington, P.R.; McCabe, P.; Pidcock, E.; Shields, G.P.; Taylor, R.; Towler, M.; van de Streek, J. Mercury: Visualization and analysis of crystal structures. *J. Appl. Cryst.* **2006**, *39*, 453–457. [[CrossRef](#)]
11. Brand, S.K.; Schmidt, J.E.; Deem, M.W.; Daeyaert, F.; Ma, Y.; Terasaki, O.; Orazov, M.; Davis, M.E. Enantiomerically enriched, polycrystalline molecular sieves. *Proc. Natl. Acad. Sci. USA* **2017**, *114*. [[CrossRef](#)] [[PubMed](#)]
12. Pace, G.G. *Zeolitas: Características, Propiedades y Aplicaciones Industriales*; Editorial Innovación Tecnológica, Facultad de Ingeniería, UCV: Caracas, Venezuela, 2000.
13. Xin, H.; Li, X.; Fang, Y.; Yi, X.; Hu, W.; Chu, Y.; Zhang, F.; Zheng, A.; Zhang, H.; Li, X. Catalytic dehydration of ethanol over post-treated ZSM-5 zeolites. *J. Catal.* **2014**, *312*, 204–215. [[CrossRef](#)]
14. Phung, T.K.; Busca, G. Diethyl ether cracking and ethanol dehydration: Acid catalysis and reaction paths. *Chem. Eng. J.* **2015**, *272*, 92–101. [[CrossRef](#)]
15. Phung, T.K.; Busca, G. Ethanol dehydration on silica-aluminas: Active sites and ethylene/diethyl ether selectivities. *Catal. Commun.* **2015**, *68*, 110–115. [[CrossRef](#)]
16. Moura, H.M.; Bonk, F.A.; Vinhas, R.C.G.; Landers, R.; Pastore, H.O. Aluminium-magadiite: From crystallization studies to a multifunctional material. *CrystEngComm* **2011**, *13*, 5428–5438. [[CrossRef](#)]
17. Vinaches, P.; Rebitski, E.P.; Alves, J.A.B.L.R.; Melo, D.M.A.; Pergher, S.B.C. Unconventional silica source employment in zeolite synthesis: Raw powder glass in mfi synthesis case study. *Mater. Lett.* **2015**, *159*, 233–236. [[CrossRef](#)]
18. Vinaches, P.; Pergher, S.B.C. Organic structure-directing agents in safo synthesis: The case of 2-ethyl-1,3,4-trimethylimidazolium. *Eur. J. Inorg. Chem.* **2018**, *2018*, 123–130. [[CrossRef](#)]
19. Rojas, A.; Cambor, M.A. A pure silica chiral polymorph with helical pores. *Angew. Chem. Int. Ed.* **2012**, *51*, 3854–3856. [[CrossRef](#)] [[PubMed](#)]

20. Villaescusa, L.A.; Márquez, F.M.; Zicovich-Wilson, C.M.; Cambor, M.A. Infrared investigation of fluoride occluded in double four-member rings in zeolites. *J. Phys. Chem. B* **2002**, *106*, 2796–2800. [[CrossRef](#)]
21. Bare, S.R.; Knop-Gericke, A.; Teschner, D.; Hävacker, M.; Blume, R.; Rocha, T.; Schlögl, R.; Chan, A.S.Y.; Blackwell, N.; Charochak, M.E.; et al. Surface analysis of zeolites: An XPS, variable kinetic energy XPS, and low energy ion scattering study. *Surf. Sci.* **2016**, *648*, 376–382. [[CrossRef](#)]
22. Collignon, F.; Jacobs, P.A.; Grobet, P.; Poncelet, G. Investigation of the coordination state of aluminum in β zeolites by X-ray photoelectron spectroscopy. *J. Phys. Chem. B* **2001**, *105*, 6812–6816. [[CrossRef](#)]
23. Gómez-Cazalilla, M.; Mérida-Robles, J.M.; Gurbani, A.; Rodríguez-Castellón, E.; Jiménez-López, A. Characterization and acidic properties of Al-SBA-15 materials prepared by post-synthesis alumination of a low-cost ordered mesoporous silica. *J. Solid State Chem.* **2007**, *180*, 1130–1140. [[CrossRef](#)]
24. Martins, L.; Cardoso, D.; Hammer, P.; Garetto, T.; Pulcinelli, S.H.; Santilli, C.V. Efficiency of ethanol conversion induced by controlled modification of pore structure and acidic properties of alumina catalysts. *Appl. Catal. A Gen.* **2011**, *398*, 59–65. [[CrossRef](#)]
25. Santos, R.C.R.; Pinheiro, A.N.; Leite, E.R.; Freire, V.N.; Longhinotti, E.; Valentini, A. Simple synthesis of Al_2O_3 sphere composite from hybrid process with improved thermal stability for catalytic applications. *Mater. Chem. Phys.* **2015**, *160*, 119–130. [[CrossRef](#)]



© 2018 by the authors. Licensee MDPI, Basel, Switzerland. This article is an open access article distributed under the terms and conditions of the Creative Commons Attribution (CC BY) license (<http://creativecommons.org/licenses/by/4.0/>).